Asian Journal of Chemistry; Vol. 26, No. 7 (2014), 2125-2128

ASIAN JOURNAL OF CHEMISTRY

http://dx.doi.org/10.14233/ajchem.2014.16499

Preparation of Nano-Crystalline $ZnMn_2O_4$ System by Sol-Gel Route

N.M. DERAZ[1,*], OMAR H. ABD-ELKADER[2,3], M.M. SELIM[1], O. EL-SHAFEY[1] and A.A. EL-ASMY[4]

[1]Physical Chemistry Department, Laboratory of Surface Chemistry and Catalysis, National Research Center, Dokki, Cairo, Egypt
[2]Zoology Department, College of Science, King Saud University, Riyadh 11451, Kingdom of Saudi Arabia
[3]Electron Microscope and Thin Films Department, National Research Center, El-Behooth Street, 12622, Giza, Egypt
[4]Chemistry Department, Faculty of Science, Mansoura University, Mansoura, Egypt

*Corresponding author: E- mail: nmderaz@yahoo.com

Received: 9 October 2013; *Accepted*: 20 November 2013; *Published online*: 22 March 2014; AJC-14975

Morphological, structural and catalytic studies of nanostructures of $ZnMn_2O_4$ powders are presented. These powders were synthesized by sol-gel method with the calcination at 400-800 °C. The phase purity and crystal structure of investigated mixed oxides are carried out by powder X-ray diffraction. Scanning electron microscopy, transmission electron microscopy and energy dispersive X-ray allowed characterizing the morphology, microstructure and surface molar composition of these nano-materials. The catalytic activity was tested for the hydrogen peroxide decomposition in aqueous solution at 30-50 °C. The effects of calcination temperature on the structural, morphological and catalytic characteristics of the investigated solids were determined. The XRD results showed that the calcination temperature affect the solid state reaction between Zn and Mn oxides. It was found that the catalysts were active depending upon the smaller particle size of the as prepared solids.

Keywords: Sol-gel, XRD, EDX, $ZnMn_2O_4$, H_2O_2-Decomposition.

INTRODUCTION

Manganese oxides with different structures have an important interest in many researches due to their particular properties and applications. Most of the structural frameworks of the manganese oxides consist of octahedral units[1]. The structural differences are commonly contributed to variations in particle size and the type of defect chemistry[2]. Since manganese oxides with different structures exhibit excellent cation-exchange and molecular adsorptive properties, they can be used as ion-sieves, molecular-sieves, catalysts and cathodic materials for lithium batteries[3-7]. Transition metal manganites were prepared by precipitation-deposition, hydrothermal or sol- gel processes[1]. The main advantage of these low temperature methods is to give solids with large specifics surface area and high porosity in the meso and macro ranges. A number of research work is being done now on alkoxide sol-gel chemistry, but these precursors are much more expensive and difficult to handle in aqueous solution[2]. Sol-gel method offers excellent control of mixing because of its ability to alter relative precursor reactivity. The principle of the synthesis is to prepare the co-gel of both metal derivatives in appropriate organic solvent by reaction with water in stoichiometric amounts, while establishing the required pH with the use of volatile bases and acids. The supercritical drying is operated with respect to the solvent exhibiting the highest critical temperature in the case when two different solvents or dispersants have been selected. Transition metal manganites have a cubic spinel structure, in which oxygen ions form a face centered cubic lattice and two different interstitial sites occupied by the cations are of two kinds as tetrahedral (A) sites and octahedral (B) sites[3]. The spinel crystal structure is only formed when the ionic radius of the cation (M) is less than about 1 Å. If it is > 1 Å, then the electrostatic coulomb forces are insufficient to ensure the stability of crystal[4].

These materials are usually synthesized by co-precipitation or sol-gel method followed by high-temperature calcination. However, specific surface areas of these spinels are usually rather low[5-11], typically not exceeding 50 m^2g^{-1}, limiting the catalytic potential of these materials.

The catalytic properties of manganese mixed oxides are attributed to the variability of the Mn oxidation state that allows the formation of oxides and their oxygen storage capacity in crystalline. An increased dispersion of MnO_x on the oxide surface leads to a significant increase in the catalytic activity, which has been attributed to a larger catalyst surface exposed to the reaction feed[12-15].

The present work reports the effect of the calcination temperature on the formation, structural, morphological and catalytic properties of zinc manganite. The characterization

techniques employed in this investigation were XRD, EDX, SEM and TEM techniques. The as prepared samples have also been tested as catalysts in the hydrogen peroxide decomposition at 30, 40 and 50 °C.

EXPERIMENTAL

The mixed oxides were prepared using sol-gel method by mixing finely powdered $MnCO_3$ (2.3 g) and $Zn(NO_3)_2{\cdot}6H_2O$ (5.8 g) in 40 mL ethylene glycol in 500 mL beaker. The mixture was boiled on a hot plate for 3 h until no yellow fumes. The precipitate was cooled, washed with ethanol, dried and calcined at 400, 600 and 800 °C for 4 h. The starting materials $Zn(NO_3)_2{\cdot}6H_2O$ was provided by Aldrich Chemical Co. while $MnCO_3$ provided from Prolabo.

Techniques: X- ray powder diffractograms (XRD) of the samples calcined at 400, 600 and 800 °C for 4 h were recorded using a Bruker diffractometer (Bruker D8 advance target) and the scan rate was fixed at 8° in 2θ min^{-1} for phase identification. The patterns were run with CuK_α with secondly monochromator (λ = 0.1545 nm) at 40 kV and 40 mA.

The crystallite sizes of ZnO and $ZnMn_2O_4$ phases were calculated from the X-ray line broading analysis of main diffraction lines of thes phases using the Scherrer equation[16]:

$$d = \frac{B\lambda}{\beta\cos\theta}$$

where, d is the mean crystallite diameter, λ is the X-ray wavelength, B is the Scherrer constant (0.89), β is the full width at Half Maximum (FWHM) of ZnO and $ZnMn_2O_4$ diffraction lines and θ is the diffraction angle of the phases under investigation.

Energy dispersive X-ray, EDX, measurements were carried out on a Hitachi S-800 electron microscope with a Kevex Delta system attached. The parameters were: -15 kV accelerates voltage, 100 s accumulation time and 8 μm windows width. The surface molar composition was determined by the Asa method (Zaf-correction, Gaussian approximation).

Transmission electron microscope observation was performed on a JEOL JEM-1230 electron microscope at accelerating voltage of 120 kV. TEM samples were deposited on thin amorphous carbon films supported on copper grids from ultrasonically processed ethylene glycol solution of the products and used to observe the morphology of the nanosized particles. A drop of the solution was placed on a copper grid that was left to dry before transferring into the TEM sample chamber.

Scanning electron microscope image was carried out for the investigated samples. Using SEM Model Philips XL 30 attached with energy dispersive X-ray unit, with accelerating voltage 30 K.V., magnification 10 x up to 400.000x and resolution for W. (3.5 nm). The samples are coated with gold.

The catalytic activates of various catalyst samples determined by studying the decomposition of H_2O_2 in the presence of these specimens at temperature within at 30-50 °C using 50 mg of a given sample with 0.5 mL of H_2O_2 of known concentration diluted to 20 mL with distilled water. The reaction kinetics was monitored by measurement the volume of oxygen gas liberated at different time interval until equilibrium was attained.

RESULTS AND DISCUSSION

X-ray diffraction: Fig. 1 displays the XRD diffractograms of Zn/Mn mixed oxides calcined at 400, 600 and 800 °C for 4 h. Inspection of this figure revealed that: (i) Zn/Mn mixed solids calcined at 400 °C consisted of well crystalline ZnO and $ZnMn_2O_4$ phases. This indicates the promotion effect of preparation method in the formation of $ZnMn_2O_4$ phase. (ii) Increasing the calcination temperature of the as prepared solids 600 °C resulted to a decrease in the peak height of ZnO phase with subsequent an increase in that of $ZnMn_2O_4$ crystallite. One can not overlook the presence of manganese oxides as amorphous phases depending upon the applied method of preparation catalyst. (iii) The calcination temperature of the as-synthesized at 800 °C is sufficient to yield $ZnMn_2O_4$ as a single phase. (iv) The peak height of $ZnMn_2O_4$ phase at 800 °C is greater than that at 400 and 600 °C.

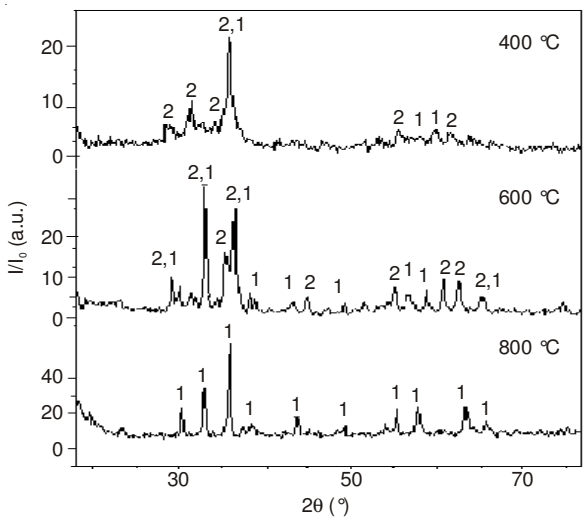

Fig. 1. XRD pattern of Zn/Mn mixed oxide calcined at different temperatures; Lines (1)) $ZnMn_2O_4$ and (2) ZnO

The degree of crystallinity and crystallite size of $ZnMn_2O_4$ phase are listed in Table-1. Investigation of Table-1 showed that: (i) the degree of crystallinity and crystallite size of $ZnMn_2O_4$ nano-particles at 800 °C are greater than[15] that at 400 and 600 °C. (ii) The crystallite size for the investigated solids prepared by sol gel method and calcined at 400, 600 and 800 °C are always smaller than those prepared by ceramic method[15]. In the light of these results, the catalytic activities of solids prepared by sol gel method should be greater than that of synthesized by ceramic method. This expectation has been verified experimentally.

Energy dispersive X-ray measurements: EDX measurements were carried out for Zn/Mn mixed oxides system calcined at 400-800 °C. The relative atomic abundance of Mn, Zn and oxygen species present in the uppermost surface layers of different solids investigated is given in Table-2. It is well known that EDX technique supplies the effective atomic concentration of different constituents of the solids investigated present on their top surface layers.

Inspection of table-2 reveled that: (i) the surface Mn/Zn ratio in the solids at 400-800 °C is strongly dependent on the calcination temperatures. (ii) The surface concentrations of

TABLE-1
CRYSTALLINTY AND CRYSTALLITE SIZE OF DIFFERENT Zn/Mn MIXED OXIDE SOLIDS AT VARIOUS CALCINATION TEMPERATURES

Samples	Calcination temp. (°C)	Crystalline phases	Degree of crystallinity (a.u.)	Crystallite size (nm)
Zn/Mn mixed oxides	400	ZnO	9.20	8.6
		$ZnMn_2O_4$	8.18	6.5
	600	ZnO	9.82	32.8
		$ZnMn_2O_4$	10.10	29.3
	800	$ZnMn_2O_4$	39.40	58.8

TABLE-2
DETERMINATION OF EDX OF THE SURFACE AND BULK MOLAR CONCENTRATION OF Zn/Mn MIXED OXIDES CALCINED AT DIFFERENT TEMPERATURES

Solids	Calcin. temp. (°C)	Elements	Atomic abundance (%)		Surface Mn/Zn Ratio
			Calculated (Bulk)	Found (Surface)	
Zn/Mn mixed oxides	400	Mn	28.4	46	2.42
		Zn	14.1	19	
		O	57.5	32	
	600	Mn	28.4	40	1.90
		Zn	14.1	21	
		O	57.5	39	
	800	Mn	28.4	36	1.33
		Zn	14.1	27	
		O	57.5	37	

Mn and Zn in all solids investigated are higher than that in the bulk of these solids. (iii) The heat treatment of the investigated mixed solids at 400 °C gave higher surface manganese/zinc ratio. Increasing the calcination temperature of the as prepared solids brought about a decrease in the surface Mn/Zn ratio. These findings suggest a possible migration of some manganese species from the surface towards the bulk of the solids parallel to the concentration gradient.

SEM and TEM investigations: The SEM photographs of Zn/Mn mixed oxides calcined at 400 and 800 °C are shown in Fig. 2a and b, respectively. It can been seen from Fig. 2 that the calcination at 400 °C led to agglomeration of nano-particles as a rock shape and also the calcination at 800 °C resulted in the same aggregation of the as prepared particles in the fragile spongy-like structure. This finding suggested that the high temperature led to decompose of spherulitic crystals into small granules with nearly sizes have flakes with loops shapes connected together make interface outlines fuzzy, but the thickness of the flakes is slightly different with different templates.

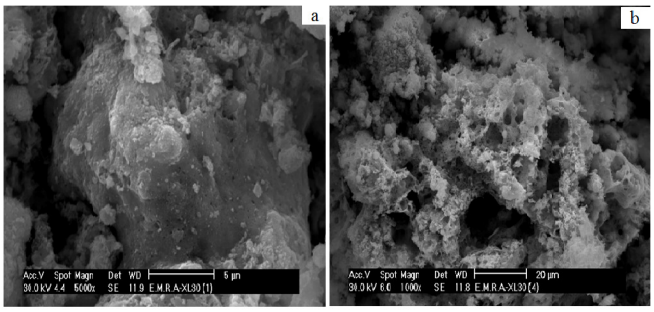

Fig. 2. SEM images of Zn/Mn mixed oxide calcined at (a) 400 °C and (b) 800 °C

Fig. 3 shows the transmission electron micrographs of mixed solids calcined at 400 °C. It is seen from this figure that the particles are spherical in shape with weak agglomerations. In the present study, the particles are ultra-fine and homogenous.

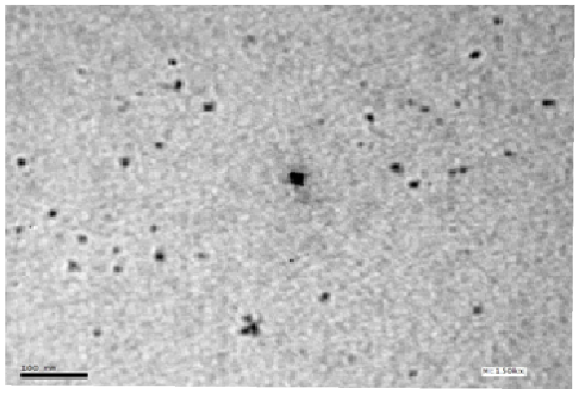

Fig. 3. TEM images of Zn/Mn mixed oxide calcined at 400 °C.

Catalytic decomposition of H_2O_2 over the prepared Zn/Mn mixed oxides system: The kinetic of H_2O_2 decomposition in the presence of various Zn/Mn mixed oxide catalysts were monitored by measuring the volume of O_2 librated at different time intervals until equilibrium was attained. Such catalytic activity were undertaken at 30, 40 and 50 °C, respectively. The results obtained showed that the reaction followed first-order kinetics in all cases. the slope of the first-order plots allowed the ready determination of the reaction rate constant, k, measured at a given temperature for a given catalyst sample. The effects the calcination temperatures on the catalytic activities of various catalysts are better investigated by comparing the values of k measured at different temperatures over different solids. The results obtained are listed in Table-3. Inspection of Table-3 revealed that: (i) the catalytic activities increase progressively as a function of the reaction temperature for all Zn/Mn mixed oxide catalysts. (ii) An increase of the calcination temperature of the investigated catalyst resulted in a decrease in its catalytic activities[15].

It has been known that the preparation temperature plays an important role in the catalytic behavior *via* the dispersion and surface concentration of active phase involved in the catalytic

TABLE-3
EFFECTS OF THE CALCINATION TEMPERATUTES ON THE REACTION RATE CONSTANT (k, sec^{-1} g^{-1}) FOR THE CATALYTIC DECOMPOSITION OF H_2O_2 DECOMPOSITION OVER THE AS PREPARED CATALYSTS

Solids	Calcination temp. (°C)	$k \times 10^3$ (sec^{-1} g^{-1})			ΔE_a (kJ/mol)
		30 °C	40 °C	50 °C	
Zn/Mn mixed oxides	400	11.5	12.45	15.64	7
	600	10.76	12.06	12.98	12
	800	8.4	11.94	11.78	13

reaction. In other words, the particle size and final local concentration of the catalytic materials are strong dependence on the calcination temperatures and the catalyst preparation method[17-30]. In fact, XRD results showed that the crystallinity and crystallite size of different oxides increases as the calcinations temperature increases. However, EDX investigations showed that the surface Mn/Zn ratio for the as prepared solids decreases as the calcinations temperature increases. These findings suggest that the dispersion of active species available for reaction decrease by increasing the calcination temperature leading to a significant decrease in the catalytic activities.

Conclusion

Single phase of nano-crystalline $ZnMn_2O_4$ particles were prepared using sol-gel methods. The XRD investigations showed that the calcination of Zn/Mn mixed oxides system at 800 °C resulted in formation of a single phase of $ZnMn_2O_4$. The crystallite sizes of the solids increase as the calcination temperature increases. EDX investigations revealed that the relative atomic abundance of Mn and Zn species present in the uppermost surface layers for investigated solids decreases as the calcinations temperature increases.. The heat treatment resulted in some changes in the microstructure, regarding grain size, porosity and the particle distribution of the as-prepared solids. The catalytic activity of sol-gel method based solids decreases by increasing the preparation temperature depending upon the crystallite size of these solids and also on the concentration of both Mn and Zn species present in the uppermost surface layer of catalyst.

ACKNOWLEDGEMENTS

This project was supported by King Saud University, Deanship of Scientific Research, College of Science Research Centre.

REFERENCES

1. R.G. Burns and V.M. Burns, Manganese Dioxide Symposium, Tokyo, vol. 2, p. 97 (1980).
2. C. Julien, M. Massot, R. Baddour-Hadjean, S. Franger and S. Bach, *Solid State Ionics*, **159**, 345 (2003).
3. Q. Feng, H. Kanoh and K. Ooi, *J. Mater. Chem.*, **9**, 319 (1999).
4. H. Cao and S.L. Suib, *J. Am. Chem. Soc.*, **116**, 5334 (1994).
5. L.Y. Chen, T. Horiuchi and T. Mori, *Appl. Catal. A*, **209**, 97 (2001).
6. G. Ferraris, G. Fierro, M. Lo Jacono, M. Inversi and R. Dragone, *Appl. Catal. B*, **45**, 91 (2003).
7. G. Fierro, M. Lo Jacono, M. Inversi, R. Dragone and G. Ferraris, *Appl. Catal. B*, **30**, 173 (2001).
8. T. Mathew, N.R. Shiju, K. Sreekumar, B.S. Rao and C.S. Gopinath, *J. Catal.*, **210**, 405 (2002).
9. J. Papavasiliou, G. Avgouropoulos and T. Ioannides, *Catal. Commun.*, **6**, 497 (2005).
10. Y. Tanaka, T. Utaka, R. Kikuchi, T. Takeguchi, K. Sasaki and K. Eguchi, *J. Catal.*, **215**, 271 (2003).
11. A. Urda, A. Herraiz, A. Redey and I.C. Marcu, *Catal. Commun.*, **10**, 1651 (2009).
12. R. Stoyanova, E. Zhecheva, R. Alc'antara and J.L. Tirado, *J. Mater. Chem.*, **16**, 359 (2006).
13. N.-A.M. Deraz, M.A. El-Sayed and A.A. El-Aal, *Adsorp. Sci. Technol.*, **19**, 541 (2001).
14. N.-A.M. Deraz, H.H Salim and A.A. El-Aal, *Mater. Lett.*, **53**, 102 (2001).
15. M.M. Selim, N.M. Deraz, O.I. Elshafey and A.A. El-Asmy, *J. Alloys Comp.*, **506**, 541 (2010).
16. B.D. Cullity, Elements of X- Ray Diffraction, Addison-Wesely, Reading, MA, edn 3 (1967).
17. R.S. Araujo, D.C.S. Azevedo, E. Rodriguez-Castellon, A. Jimenez-Lopez and C.L. Cavalcante Jr., *J. Mol. Catal.*, **281**, 154 (2008).
18. W.Y. Jung, S.H. Baek, J.S. Yang, K.-T. Lim, M.S. Lee, G.-D. Lee, S.S. Park and S.-S. Hong, *Catal. Today*, **131**, 437 (2008).
19. T. Vrålstad, G. Øye, M. Rønning, W.R. Glomm, M. Stöcker and J. Sjöblom, *Micropor. Mesopor. Mater.*, **80**, 291 (2005).
20. M. Zhou, J. Yu and B. Cheng, *J. Hazard. Mater. B*, **137**, 1838 (2006).
21. J. Panpranot, J.G. Goodwin Jr. and A. Sayari, *Catal. Today*, **77**, 269 (2002).
22. L.C.A. Oliveira, R.M. Lago, J.D. Fabris and K. Sapag, *Appl. Clay Sci.*, **39**, 218 (2008).
23. F. Bertinchamps, C. Grégoire and E.M. Gaigneaux, *Appl. Catal. B*, **66**, 10 (2006).
24. D. Song and J. Li, *J. Mol. Catal.*, **247**, 206 (2006).
25. H. Ming and B.G. Baker, *Appl. Catal. A*, **123**, 23 (1995).
26. G. Boudjahem, S. Monteverdi, M. Mercy and M.M. Bettahar, *J. Catal.*, **221**, 325 (2004).
27. Y. Khodakov, V.L. Zholobenko, R. Bechara and D. Durand, *Micropor. Mesopor. Mater.*, **79**, 29 (2005).
28. Y. Okamoto, K. Nagata, T. Adachi, T. Imanaka, K. Inamura and T. Takyu, *J. Phys. Chem.*, **95**, 310 (1991).
29. A.Y. Khodakov, R. Bechara and A. Griboval-Constant, *Appl. Catal. A*, **254**, 273 (2003).
30. A. Szegedi, M. Popova, V. Mavrodinova and Ch. Minchev, *Appl. Catal.*, **338**, 44 (2008).